Persistent increases in nighttime heat stress from urban expansion despite heat island mitigation

Kangning Huang[1,2*], Xuhui Lee[1], Brian Stone Jr.[2], Jason Knievel[2], Michelle L. Bell[1], and Karen C. Seto[1]

1. School of the Environment, Yale University, New Haven, CT, USA.
2. Research Application Laboratory, National Center for Atmospheric Research, Boulder, CO, USA.
3. School of City and Regional Planning, Georgia Institute of Technology, Atlanta, GA, USA.

Corresponding author: Kangning Huang (kangning.huang@yale.edu; knhuang@ucar.edu)

Abstract

Urban areas generally have higher near-surface air temperature and lower air humidity than rural areas. Little is known about how heat stress, the combined effect of high air temperature and high humidity on human physiology, will be affected by future urban land expansion. Here we use a mesoscale numerical weather prediction model to examine the effects of urban land expansion from 2000 to 2050 on heat stress (measured as wet-bulb globe temperature, WBGT) in the urban areas of China, India, and Nigeria, which are projected to account for one-third of global urban population growth through 2050. Our results show that urban expansion slightly reduces heat stress during the day (~0.2°C) but substantially intensifies it at night, by ~1°C on average and by up to 2–3°C in five mega-urban regions (MURs). These effects exist with or without climate change induced by rising concentrations of greenhouse gases (GHGs). Installing cool roofs—an urban heat island mitigation measures—can reduce the daytime WBGT by 0.5–1°C, partially offsetting the heat stress conditions caused by GHG-induced climate change. However, even with cool roofs, the nighttime WBGTs are higher by 0.3–0.9°C over the whole countries studied, and by 1–2°C in the MURs under the urban expansion scenario, compared to the situation in which urban areas remain unchanged. These results show that future urban expansion and heat island mitigation can result in potential daytime benefits but also persistent nighttime risks.

1   Introduction

Human bodies cannot effectively cool off through sweating if air temperature and humidity are high, and therefore both variables need to be accounted for in assessing the heat stress on human (Sherwood & Huber, 2010). However, despite a growing body of literature on how both variables are affected by climate change induced by greenhouse gases (GHGs) (Ahmadalipour & Moradkhani, 2018; Fischer & Knutti, 2013; Im et al., 2017; Kang & Eltahir, 2018; J. Li et al., 2018; Matthews et al., 2017; Pal & Eltahir, 2016; Sherwood & Huber, 2010), existing studies on the climatic effects of future urban land expansion primarily focus on rising air temperature (L. Chen & Frauenfeld, 2016; Georgescu et al., 2014; K. Huang et al., 2019; Krayenhoff et al., 2018) but largely overlook changes in humidity. Under humid conditions, while the removal of vegetation by urban expansion raises air temperature by reducing evaporative cooling (Oke, 1982), the reduction of evapotranspiration (ET) also diminishes

44   humidity (Adebayo, 1991; Luo & Lau, 2019; Um et al., 2007) (Figure 1). These warming and
45   drying effects also exist in arid climates, although they as not as pronounced—and sometime
46   inverted—because the ET from native arid/semi-arid vegetation is generally weaker than that
47   from urban green space. In humid climates, previous studies showed that humidity is lower in
48   existing urban areas compared to the surrounding rural areas (Ackerman, 1987; D. O. Lee,
49   1991), and that the process of urban land expansion can further reduce humidity (Adebayo, 1991;
50   Luo & Lau, 2019). What remains unknown, however, is whether the two opposing processes—
51   warming and drying—associated with future urban expansion will combine to intensify or to
52   weaken heat stress. This question is important in the context of the world's rapidly growing
53   urban population, which is anticipated to reach 6.7 billion by 2050.

54

55   Here we combine the Weather Research and Forecasting (WRF) regional numerical
56   weather prediction (NWP) model (Miao & Chen, 2014; Skamarock et al., 2008) and the spatially
57   explicit projections of urban land expansion through 2050 by (K. Huang et al., 2019), to
58   investigate the effects of urban expansion on heat stress intensity. Our index for heat stress is a
59   modified wet-bulb globe temperature (WBGT) at 2m above ground level. Compared to other
60   heat stress indices, heatwaves defined using WBGT have stronger correlations with health
61   impacts (Heo & Bell, 2018). We choose the entire countries of China, India, and Nigeria as the
62   study regions, because one-third of global urban population growth in the next three decades is
63   projected to occur there (UN DESA, 2014), and urban land areas there will expand by 40 million
64   hectares, which is about 27% of the world's total urban land expansion (K. Huang et al., 2019).
65   Heat stress in these regions is projected to rise to dangerous levels due to GHG-induced climate
66   change (Ahmadalipour & Moradkhani, 2018; Im et al., 2017; Kang & Eltahir, 2018), but we do
67   not know if the expected enormous urban expansion will further intensify the heat stress. To
68   examine the possible nonlinear interaction (Krayenhoff et al., 2018) between global climate
69   change and urban expansion, we force the WRF simulations with two sets of background climate
70   conditions: a historical climate in 2000, and a projected climate in 2050 under the representative
71   concentration pathway (RCP) 8.5 scenario (Bruyere et al., 2015; Vuuren et al., 2011). The effects
72   of two infrastructure-based urban heat island mitigations—green and cool roofs installments—
73   are evaluated in additional simulations, to explore a larger range of possible heat stress outcomes
74   in urban areas. By exploring these scenarios, we aim to answer the question of how urban land
75   expansion and heat island mitigation will contribute to changing future heat stress.

76   **2   Methods**

77   2.1   Heat stress calculation.

78   Our metric for heat stress is a modified wet-bulb globe temperature (WBGT) at 2m above
79   ground level (Dunne et al., 2013):

$$WBGT = 0.7 \times T_w + 0.3 \times T_g$$

80   wherein T_g is black globe temperature and T_w is natural wet-bulb temperature. Modifying
81   WBGT by ignoring direct sunlight and wind, T_g can be approximated by dry air temperature T_a
82   at 2m. Wet-bulb temperature T_w at 2m can be calculated by solving the equation below (X. Lee,
83   2018; Monteith & Unsworth, 2013):

$$e = e_s(T_w) - \gamma(T_a - T_w)$$

84   wherein e is water vapor pressure, $e_s(*)$ is the saturated (i.e. equilibrium) water vapor
85   pressure as a function of temperature, and γ is the psychrometer constant that depends on air
86   pressure and temperature. A numerical method provided in the R package Bigleaf (version 0.6.5)
87   is used to solve T_w (Knauer et al., 2018). Hereafter we omit "modified" when referring to
88   WBGT.

89   We choose WBGT as the metric for heat stress because it is widely accepted and used
90   (d'Ambrosio Alfano et al., 2014; Blazejczyk et al., 2012). WBGT is used in the fields of
91   industrial hygiene (Lucas et al., 2014), the military (Patel et al., 2013), and sporting (Brocherie &
92   Millet, 2015). More importantly, a recent study comparing different heat stress metrics showed
93   that WBGT is the best indicator of heat-related health impacts, such as hospitalization and heat
94   disorders during heatwaves (Heo et al., 2019).

95   2.2   Atmospheric modeling.

96   To simulate the effects of urban land expansion on both air temperature and humidity, we
97   use the advanced research version of the weather research and forecasting model (WRF, version
98   3.8) coupled with a single-layer urban canopy module (UCM) (D. Li et al., 2014; Miao & Chen,
99   2014; Skamarock et al., 2008). As a mesoscale physical-based NWP model, WRF can examine
100   the effects of land cover / land use changes—conversion to urban areas from others—on both air
101   temperature and humidity. To provide the initial and boundary conditions for WRF, we use the
102   global bias-corrected climate model output from the Community Earth System Model (CESM),
103   with historical and future GHG concentration (Bruyere et al., 2015). The future climate
104   conditions are based on the Representative Concentration Pathway (RCP) 8.5, which will result
105   from the business-as-usual, fossil-fueled economic development. To account for inter-annual
106   fluctuations, we run the simulations for five summers: 1999–2004 for current climate, and 2049–
107   2054 for future climate. When analyzing the hourly outputs from WRF, we categorize all hours
108   with positive incoming shortwave radiation as daytime, and those with zero shortwave radiation
109   as nighttime. By using incoming shortwave radiation rather than fixed hours to categorize diurnal
110   hours, we account for the different summer daytime lengths across different latitudes. The WRF
111   modeling domains over China, India, and Nigeria are shown in Figure 2.

112   2.3   Urban land expansion and heat island mitigation.

113   Future urban areas are obtained from a spatially explicit probabilistic projections of urban
114   expansion by 2050 (K. Huang et al., 2019). The urban expansion in the Shared Socioeconomic
115   Pathway 5 (fossil-fueled development) scenario is used, in order to match with the high emission
116   RCP8.5 climate change scenario. Following (L. Chen & Frauenfeld, 2016), we assume locations
117   with >75% likelihood to be urbanized by 2050 as urban areas. Following previous studies on the
118   climatic impacts of large-scale urban land expansion (L. Chen & Frauenfeld, 2016; Georgescu et
119   al., 2014; Krayenhoff et al., 2018), we run the model at 25 km horizontal grid spacing. We use
120   the global databases of urban extent and characteristics provided by (Jackson et al., 2010) to set
121   up the urban areas' parameters, such as impervious/pervious surfaces ratios, building heights,
122   street widths, heat capacity, and surface albedo. The key urban parameters of the study countries
123   are listed in Table S1. Among the study countries, urban areas in China have the highest height-
124   to-width ratio (1.8), resulting in deeper urban canyons and absorbing of more outgoing long-

125 wave radiation compared urban areas in the other two countries. Urban areas in India have the
126 lowest roof albedo, which leads to absorption of more incoming short-wave radiation. Compared
127 to those in India, urban areas in China and Nigeria have higher thermal conductivity, which can
128 increase daytime heat storage and thus stronger nighttime heat release.

129   We follow (Georgescu et al., 2014) to set up the cool roofs adaptation scenario as the
130 albedo of building rooftops being raised to 0.8. Albedo of building walls and pavements are kept
131 the same in the albedo adaptation scenario, because glare from highly-reflective walls and
132 pavements can cause visibility problems for drivers and pedestrians (Stone, 2012). The green
133 roofs adaptation option is readily available in WRF-v3.8, which includes an UCM that enables
134 modeling vegetation irrigation in urban canyons. Both cool and green roofs adaptations assume a
135 100% deployment on all available roof tops. Although these adaptations scenarios may not be
136 realistic in terms of implementation, we aim to examine the system boundaries of the urban-
137 climate-adaptation interactions regarding heat stress. Installing green or cool roofs can reduce
138 building energy consumption and thus the anthropogenic heat (AH) released in urban areas.
139 However, this feedback between adaptations and AH is not captured here, because the current
140 version of WRF-UCM does not allow simultaneously simulating building energy use and green
141 roof adaptation (J. Yang, Wang, Chen, et al., 2015). Instead, following (L. Chen & Frauenfeld,
142 2016; Georgescu et al., 2014), we implement a simple diurnal profile of anthropogenic heating
143 (Figure S2). This implementation of AH may underestimate warming from urban expansion as
144 indoor cooling systems are installed in more buildings, and it may underestimate cooling from
145 urban adaptations as green or cool roofs reduce energy used by indoor cooling. Moreover, this
146 implementation also ignores the spatial heterogeneity of anthropogenic heating, as shown in (F.
147 Chen et al., 2016; B. Yang et al., 2019). To incorporate spatial heterogenous AH in WRF
148 simulations, the input land use data need to include the spatial distributions of urban areas with
149 various densities, which are not available in the urban expansion forecasts (K. Huang et al.,
150 2019). The spatially uniform AH profiles used here may lead to underestimation of warming in
151 the denser areas near city centers.

152   When presenting the modeling results of changing WBGT in Figure 3, we categorize
153 urban areas into humid and arid. Instead of using the conventional aridity index (the ratio of
154 precipitation to potential evapotranspiration), here we use the difference in summertime average
155 evapotranspiration (ET) before and after urban land expansion to distinguish humid or arid urban
156 areas. If the average ET declines after urban expansion, urban area is removing humidity on an
157 originally humid landscape; on the contrary, if ET increases after urban expansion, urban area is
158 introducing more humidity via urban greenspace that evaporate and transpire more vapor than
159 the native arid vegetation. We use this definition because it can better reflect the different roles
160 urban land expansion play under different climate conditions. The geographic distributions of
161 humid and arid urban areas are shown in Figure 2. When presenting the results across
162 geographies (Figure 4) and on the temperature-humidity-plane (Figure 5), we overlay them on
163 the present Köppen climate zones provided in (Beck et al., 2018). With the labels of Köppen
164 climate zones, we can show which MURs are located in the transition zones (e.g. Beijing and
165 Delhi) and show the differences among various types of humid urban areas.

166 2.4   Model validation.

167   To validate the model's capabilities in simulating the diurnal variations of air
168 temperature, humidity, and heat stress, we compare the simulated results with the observations

169   obtained from the integrated surface database (ISD) from the National Oceanic and Atmospheric
170   Administration (Smith et al., 2011). ISD provides hourly meteorological observations with
171   global coverage. In total, 404 ISD stations in China, 408 in India, and 40 in Nigeria are used in
172   the validation. The validation shows that the simulated values agree with the observed ones
173   sufficiently well for air temperature (Figure S4; R^2=0.74), relative humidity (Figure S5;
174   R^2=0.56), and wet-bulb temperature (Figure S6; R^2=0.82). To better evaluate the model's
175   performance in urban areas, the correlation coefficients (R^2's) shown here are calculated with
176   grid cell samples weighted by their fraction of urban land.

177   ## 3   Results

178   Our results show that in 2050 urban land expansion and heat island mitigation have
179   diurnally different impacts on WBGT in the urban areas of the three countries. Urban expansion
180   slightly reduces WBGT in the daytime, by 0.1–0.3°C, but substantially increases WBGT at
181   night, by 0.5°C in India, and more than 1°C in China and Nigeria (Figure 3-a). Compared to
182   India, the stronger nighttime urban warming in China and Nigeria is caused by the higher
183   thermal conductivity of the building materials, which increases heat storage during daytime and
184   releases more heat at night. Both urban heat island mitigation measures—installation of green
185   and cool roofs—can reduce heat stress, although the latter is more effective than the former. The
186   combination of urban land expansion and heat island mitigation leads to a total reduction in
187   daytime WBGT by 1.2°C in China, and 0.6–0.7°C in India and Nigeria. At night, however,
188   neither mitigation measures can fully counteract the heat stress increases from urban expansion;
189   the net effect is an increase of 0.2–0.3°C in the nighttime WBGT in China and India and of
190   ~0.9°C in Nigeria. If we restrict the analysis to urban areas in the arid regions, we find that urban
191   land expansion has little effect on WBGT both during the daytime (<0.1°C) and nighttime
192   (<0.3°C), and urban heat island mitigation measures are only half as effective as those in the
193   humid regions (Figure 3-b).

194

195   The most severe increases in nighttime urban heat stress are concentrated in several
196   population centers that already face substantial challenges in climate change adaptation.
197   Although nighttime WBGT increases by less than 1°C in most urban areas from 2000 to 2050,
198   the increase is much larger, by 2–3°C, in five hotspot mega-urban regions (MURs; Figure 4): A)
199   Beijing-Tianjin-Hebei, located in the transition zone between cold and arid climates of northern
200   China; B) Yangtze-River-Delta, in the temperate climate of eastern China, in the lower reaches
201   of Yangtze River; C) Chengdu-Chongqing, in the temperate climate of southern China, in the
202   middle reaches of Yangtze River; D) Delhi Metropolitan Area, in the transition zone between
203   arid and temperate climates of northwestern India; and E) Port Harcourt, in the tropical coast of
204   southern Nigeria. Even if cool roofs are installed, 1–1.5°C nighttime warming will remain in
205   Yangtze-River Delta, Chengdu-Chongqing, and Delhi Metropolitan Area, and up to 2°C in
206   Beijing-Tianjin-Hebei and Port Harcourt.

207

208   Owing to their various geographic conditions, these hotspot MURs will face different
209   challenges in coping with the increasing urban heat stress. Beijing-Tianjin-Hebei and Delhi
210   Metropolitan Area, two MURs located in the transition zones toward arid climates, face more
211   severe water shortage due to accelerated dryland expansion (J. Huang et al., 2016) and depleted

212   groundwater (J. Chen et al., 2014; Feng et al., 2013). Although the water-demanding green roofs
213   are less effective as shown here, water resources are still needed to support street trees, which
214   can mitigate heat stress by providing shade (Coutts et al., 2016)—a cooling strategy that is not
215   included in our analysis. In Beijing-Tianjin-Hebei, the more effective cool roofs installment can
216   lead to lower temperature in winter, increasing the cold-related health risks (Gasparrini et al.,
217   2015) and building energy consumption (J. Yang, Wang, & Kaloush, 2015). The other three
218   MURs (Yangtze-River Delta, Chengdu-Chongqing and Port Harcourt) rarely have water
219   shortages or cold winters, but will experience more extreme heat events due to GHG-induced
220   climate change. Annual heatwave days in the middle and lower reaches of Yangtze River, which
221   includes Yangtze-River Delta and Chengdu-Chongqing, will increase from less than 10 now to
222   ~80 by the end of 21st century, under the RCP8.5 scenario (Guo et al., 2017). Under this high
223   emission scenario, heat stressed days in western Africa, which includes the Port Harcourt MUR,
224   will increase from ~50 now to ~200 by the 2090s (Rohat et al., 2019). The persistent increases in
225   nighttime urban heat stress shown here will likely further exacerbate the heat-related risks in
226   these three MURs. Since previous studies showed that socioeconomic factors also affect
227   residents' vulnerabilities to heat risks (Hu et al., 2017, 2019), we further distinguish the heat
228   stress-related challenges in these MURs by comparing their income-levels by 2050. Table 2
229   shows the average GDP per capita by 2050 in the five MURs, calculated from the spatially
230   gridded forecasts of population and GDP by (Murakami & Yamagata, 2019) (Figure S3). With
231   GDP per capita higher than 30,000 (USD 2005), urban residents in the three MURs in China are
232   less vulnerable to increasing heat stress. With GDP per capita of ~15,000 in Delhi Metropolitan
233   Area and ~10,000 in Port Harcourt, urban residents in these two MURs will have higher
234   challenges in heat stress adaptations. In these two MURs, government assistance in mitigating
235   urban heat and providing heat shelters will be more critical. Moreover, given that cool roofs are
236   less expensive than green roofs to install (Estrada et al., 2017), this adaptation should be given
237   higher priority for the low-income households in these two MURs. Although green roofs are less
238   effective in mitigating heat stress and are more expensive, they can provide ecological benefits
239   (Williams et al., 2014) that may be needed in Port Harcourt, whose future expansion will
240   threaten the biodiversity hotspot of Western African Forests (Myers et al., 2000; Seto et al.,
241   2012).

242

243   To illuminate the mechanisms of the diurnally differentiated results shown above, Figure
244   5 disentangles the effects of urban land expansion (a–b) and heat island mitigation (c–d) on air
245   temperature (x-axis) and relative humidity (y-axis), under the future climate conditions (2049–
246   2055, RCP8.5). In these plots, each arrow indicates the mean change from 2000 to 2050 of urban
247   areas located in a Köppen climate zone, and dashed lines are contours of WBGT. Urban land
248   expansion raises daytime air temperature but reduces relative humidity in all climate zones
249   except for arid hot desert climate (BWh), as indicated by the arrows pointing toward the lower-
250   right directions (Figure 5-a). The arrows in the temperature-humidity-plane are mostly parallel
251   to the contour lines of WBGT, meaning that the drying effects of urban expansion largely offset
252   its warming effects and the result is little change in the daytime WBGT. During nighttime
253   (Figure 5-b), however, most arrows cross the contour lines to the right, or in other words
254   warming overwhelms drying, which results in WBGT increases. This diurnal asymmetry in heat
255   stress changes is mainly due to the diurnally asymmetric effects of urban expansion on warming
256   and drying. Table 1 shows that, in most climate zones, urban expansion raises air temperature
257   more during nighttime than daytime, but it reduces specific humidity more during daytime than

6

258   nighttime. The nighttime increase in air temperature is stronger because the replacement of rural
259   landscape with urban area shifts daytime sensible and latent heat fluxes to heat storage, which is
260   released at nighttime. The daytime decrease in specific humidity is stronger because the
261   replacement of vegetated landscape with impervious urban area significantly reduces ET during
262   daytime; whereas at night, the drying effect is weaker since there is little ET to be reduced.

263

264   Urban heat island mitigation measures (Figure 5 c & d) reduce air temperature but
265   increase humidity, which is not surprising for green roof installment whose evaporative cooling
266   adds extra moisture into the atmosphere. What may seem counterintuitive is that cool roof
267   installment, which reduces surface solar radiation absorption by increasing albedo, also raises
268   humidity. This drying effect of cool roofs can be explained by the evolution of atmospheric
269   boundary layer (ABL) (X. Lee, 2018). In this cool-roof scenario, less solar radiation energy is
270   available to drive convection and as a result the ABL is shallower (Epstein et al., 2017),
271   concentrating in a smaller volume the water vapor that originates at the ground, thereby
272   increasing humidity.

273

274   To determine whether the diurnal and geographic variations presented above will be
275   affected by global climate change, we repeat the model calculation with two sets of boundary
276   conditions (invariant urban areas versus urban expansion scenario) and two GHG scenarios (one
277   in current climate and another in future climate under RCP 8.5), for a total of four permutations.
278   Figure S1 shows the changes in WBGT due to urban expansion under current (1999–2004; y-
279   axis) and future (2049–2054, RCP 8.5; x-axis) climate conditions. Under both climate
280   conditions, urban expansion results in daytime cooling (left panel) and nighttime warming (right
281   panel) for 68.2% and 70.5% of urban areas in 2050, respectively. Across geographic locations,
282   WBGT changes under the two climate conditions are strongly correlated ($R^2 = 0.85$ in daytime
283   and 0.91 in nighttime). These results suggest that nonlinear interactions between urban expansion
284   and GHG emission are nearly negligible and that the overall effect can be estimated by linearly
285   adding the effects from urban expansion and the effects from GHG emission. These results may
286   seem contradictory to a recent study that showed nonlinear interactive effects on surface air
287   temperature between urban expansion and GHG emission (Krayenhoff et al., 2018). This
288   apparent contradiction arises mostly from the fact that the WBGT change has accounted for both
289   temperature change and humidity change. The interaction between GHG emission and urban
290   expansion can be defined as the difference of urban expansion-induced changes under future and
291   current climate conditions. We quantified the interactive effects on air temperature (T_a), relative
292   humidity (RH), and WBGT, during the daytime (Table S1) and nighttime (Table S2), in seven
293   climate zones where the majority of future urban areas will be located. The interactive effects on
294   T_a and RH are the opposite, resulting in little change in WBGT, in urban areas in the tropical
295   savannah (Aw), arid (BSh & BSk), humid subtropical (Cwa) and continental (Dwb) climates,
296   accounting for about 76% of all urban areas in 2050 of our study regions. Our analysis suggests
297   that, for a large portion of future urban areas, it is possible to superimpose the effects on heat
298   stress from urbane expansion presented here on those from climate change under other GHG
299   scenarios, when projecting future heat stress on urban residents.

4   Discussions

Using atmospheric modeling and urban expansion projections and by combining air temperature and humidity predictions, we reveal a diurnal pattern of future urban heat stress that has been missing in existing literature. Our results show that urban expansion increases heat stress (quantified as modified WBGT in this paper) much more at night than during the day. Our results also show that urban heat island mitigation measures have the potential to reduce daytime heat stress but bring little change to nighttime stress (Figure 3).

Increasing urban heat stress can amplify health risks and energy consumptions. The persistent nighttime urban warming revealed herein suggests heat mitigation measures need to prioritize residential buildings, where most urban dwellers spend the night. There is evidence that, compared to daytime, exposure to nighttime extreme heat contributes more to mortality risks, especially in urban areas (Laaidi et al., 2011; Murage et al., 2017). In less extreme conditions, hotter nights nevertheless still disrupt sleep patterns (Obradovich et al., 2017), leading to physiological and psychological harms. While most of the heat-health effects studies are based on only air temperature, there is emerging empirical evidence (Heo et al., 2019; Heo & Bell, 2018) showing that heat stress indices that account for humidity can better explain the health outcomes. However, these heat-related health impact studies focus either on nighttime air temperature or daytime heat stress, providing limited understanding on the quantitative relationship between nighttime heat stress and health. Further studies on the health impacts of nighttime heat stress are needed, in the manner of this study, in order to better understand how urban expansion might threaten human health.

One of the most effective ways to reduce heat stress is by cooling indoor spaces. However, according to a recent projection by International Energy Agency (IEA, 2018) that includes both temperature and humidity, energy demands for indoor cooling will increase threefold from 2,020 terawatt-hours (TWh) in 2016 to 6,200 TWh in 2050, accounting for 30% of the global building electricity use. This IEA projection incorporates future population and economic growth, and a 1°C GHG-induced global warming, but ignores the warming caused by urban expansion. Without considering urban expansion-warming, it is projected that about 70% of the increase in global cooling energy use will come from the residential sector, and that China and India will account for more than half of the global expansion in the capacity of residential indoor cooling. The urban expansion-induced nighttime WBGT increases associated with urban expansion showed here imply an underestimation in the IEA cooling energy use projection that only considers GHG emissions. Since most urban residents spend the nights at home, our results expansion-induced nighttime warming of WBGT in China and India indicate that future cooling energy use will be substantially higher than the existing projection. According to the assumption that a 1°C warming corresponds to 25% increase in cooling loads used in the IEA projection, our result of ~1°C nighttime WBGT warming in China and India suggests that the energy used for cooling their cities at night will probably be higher by about a quarter. Since indoor cooling also intensifies UHI by releasing waste heat, future modeling research accounting for the interactions between heat stress, urban expansion, and indoor cooling is still needed to reliably quantify future urban expansion's impact on energy use.

344   The potential impacts on human health and energy use discussed above demonstrate the
345   needs to mitigate future increase in nighttime heat stress caused by urban expansion. However,
346   our results show that infrastructure-based urban heat island (UHI) mitigation measures—
347   installing green/cool roofs—can increase relative humidity via increasing surface evaporation
348   (green roofs) or suppressing the atmospheric boundary layer (cool roofs), making those forms of
349   mitigation less effective in reducing WBGT (Figure 3 and Figure 5). Our analysis suggests that
350   even if green/cool roofs are deployed at a large-scale, these UHI mitigation measures can only
351   reduce about half of the urban expansion-induced increase in nighttime heat stress. Mitigating
352   the persistent nighttime heat stress in the rapidly expanding Asian and African cities will require
353   multi-disciplinary solutions beyond the green/cool roofs often examined in atmospheric studies
354   (Georgescu et al., 2014; Stone et al., 2014; Zhao et al., 2017). One possible complementary
355   strategy against nighttime urban heat stress is improving insulation of residential buildings. Since
356   cool roofs have been shown to reduce indoor heat stress by 26–46% (Zinzi & Agnoli, 2012),
357   improved building insulation can prevent the persistent half of outdoor WBGT increase from
358   compromising indoor thermal comfort. Because the ~0.4 million km^2 of future urban areas in
359   China, India and Nigeria do not exist now and will be built in the next decades (K. Huang et al.,
360   2019), establishing regulations on cool roofs and residential building insulation can generate
361   potential benefits of heat stress mitigation for ~8 million additional urban residents in these
362   countries by 2050 (UN DESA, 2014).

363

364   Our results show that the combination of urban land expansion and heat island mitigation
365   has the potential during daytime to reduce heat stress, providing an opportunity to delay un-
366   inhabitable climate conditions. Due to global climate change under the RCP 8.5 scenario, by the
367   end of 21st century, daily maximum heat stress in northeastern South Asia and eastern China will
368   approach or exceed the critical threshold of 35°C wet-bulb temperature, beyond which human
369   bodies cannot sufficiently cool off by sweating (Im et al., 2017; Kang & Eltahir, 2018). Because
370   extreme heat stress usually occurs in the afternoon (C. Raymond et al., 2017), our results
371   regarding daytime urban cooling, suggest that urban expansion by 2050, with cool roofs
372   installed, can potentially delay the exceedance of critical heat stress thresholds, allowing extra
373   time for GHG emission mitigation or strategic retreat from those un-inhabitable regions.
374   However, since observed heat stress extremes are mainly driven by horizontal transport of
375   moisture (C. Raymond et al., 2017; Colin Raymond et al., 2020), it is unclear whether the local
376   drying effects of urban expansion are strong enough to counteract moisture advection. Further
377   modeling studies to investigate the interaction between urban expansion and moisture transport
378   are still needed to understand the potential benefits of avoiding exceedance of heat stress
379   thresholds. In less extreme conditions, WBGT higher than 25°C, albeit not lethal, can lead to
380   labor capacity loss in outdoor environments. Even if GHG-induced global warming is limited to
381   a 2°C change from pre-industrial level, global labor capacity loss, especially in low- to mid-
382   latitudes, will more than double from 10% now to 25% by 2050 due to rising heat stress (Dunne
383   et al., 2013). Our result of ~1°C reduction in daytime WBGT from combining urban expansion
384   and adaptation shows the potential to alleviate labor productivity loss in urban areas. Improving
385   outdoor labor productivity will be critical in maintaining the gray urban infrastructures, such as
386   pavements and power supplies, whose degradation has been projected to accelerate with global
387   climate change (Forzieri et al., 2018; Underwood et al., 2017).

388

389   One important caveat of our analysis is the inadequate representation of shade and wind
390 in our quantification of heat stress and atmospheric modeling. In addition to air temperature and
391 humidity, thermal comfort is also affected by the direct solar radiation on human bodies, which
392 can be reduced by shading (Harlan et al., 2006). Our analysis cannot adequately address the
393 shading effects for two reasons. First, shading depends on various urban form factors, such as
394 building heights, street widths, and tree canyons. Accounting for variations in urban forms
395 requires analyses that are beyond the scope of this paper—the effects of adding new urban areas
396 with similar structures to the existing ones. Second, the tree-canopy representation in the WRF
397 model does not adequately capture the cooling effects from shading (Wang et al., 2016). To
398 address this caveat, multiple scenarios of various urban forms and an improved urban-canyon-
399 tree-canopy model need to be included in future studies. Nonetheless, considering the shading
400 effects, it is reasonable to speculate that urban forms with narrower streets and more street trees
401 have the potential to further reduce daytime heat stress.

402 **5   Conclusions**

403   The climate is changing and the world is urbanizing rapidly. Both processes can
404 potentially increase heat stress in urban areas, yet the effects of urban expansion remain unclear.
405 Our results, from simulating the effects of urban expansion on both temperature and humidity,
406 reveal a new diurnal pattern of changing heat stress. During daytime conditions, urban land
407 expansion and heat island mitigation provide the opportunity to delay extreme heat conditions
408 caused by climate change. During nighttime conditions, the persistent warming at night can
409 exacerbate increases in health risks and energy consumption, which requires complementary
410 measures like combining green/cool roofs with improved building insulation.

411

418 **Data Availability Statement**

419   The results of nighttime WBGT increases are available for download at figshare
420 (https://figshare.com/s/9b991f83366a29c45e09 and
421 https://figshare.com/s/0d61755f759d40d5bc6f). Full WRF outputs are not deposited on public
422 data repository due to the large file sizes. These outputs are available upon request from the
423 correspondence author K. Huang. Other data needed to run the simulations include: the spatially
424 explicit, probabilistic forecasts of global urban land expansion by 2050
425 (https://doi.org/10.6084/m9.figshare.7897010) and the NCAR CESM Global Bias-Corrected
426 CMIP5 Output to Support WRF/MPAS Research (https://rda.ucar.edu/datasets/ds316.1/).

References

Ackerman, B. (1987). Climatology of Chicago Area Urban-Rural Differences in Humidity. *Journal of Climate and Applied Meteorology*, *26*(3), 427–430. https://doi.org/10.1175/1520-0450(1987)026<0427:COCAUR>2.0.CO;2

Adebayo, Y. R. (1991). Day-time effects of urbanization on relative humidity and vapour pressure in a tropical city. *Theoretical and Applied Climatology*, *43*(1–2), 17–30. https://doi.org/10.1007/BF00865039

Ahmadalipour, A., & Moradkhani, H. (2018). Escalating heat-stress mortality risk due to global warming in the Middle East and North Africa (MENA). *Environment International*, *117*, 215–225. https://doi.org/10.1016/j.envint.2018.05.014

d'Ambrosio Alfano, F. R., Malchaire, J., Palella, B. I., & Riccio, G. (2014). WBGT Index Revisited After 60 Years of Use. *The Annals of Occupational Hygiene*, *58*(8), 955–970. https://doi.org/10.1093/annhyg/meu050

Beck, H. E., Zimmermann, N. E., McVicar, T. R., Vergopolan, N., Berg, A., & Wood, E. F. (2018). Present and future Köppen-Geiger climate classification maps at 1-km resolution. *Scientific Data*, *5*, 180214. https://doi.org/10.1038/sdata.2018.214

Blazejczyk, K., Epstein, Y., Jendritzky, G., Staiger, H., & Tinz, B. (2012). Comparison of UTCI to selected thermal indices. *International Journal of Biometeorology*, *56*(3), 515–535. https://doi.org/10.1007/s00484-011-0453-2

Brocherie, F., & Millet, G. P. (2015). Is the Wet-Bulb Globe Temperature (WBGT) Index Relevant for Exercise in the Heat? *Sports Medicine*, *45*(11), 1619–1621. https://doi.org/10.1007/s40279-015-0386-8

Bruyere, L., Monaghan, J., Steinhoff, F., & Yates, D. (2015). Bias-Corrected CMIP5 CESM Data in WRF/MPAS Intermediate File Format. https://doi.org/10.5065/D6445JJ7

451   Chen, F., Yang, X., & Wu, J. (2016). Simulation of the urban climate in a Chinese megacity with

452   spatially heterogeneous anthropogenic heat data. *Journal of Geophysical Research:*

453   *Atmospheres*, *121*(10), 5193–5212. https://doi.org/10.1002/2015JD024642

454   Chen, J., Li, J., Zhang, Z., & Ni, S. (2014). Long-term groundwater variations in Northwest India

455   from satellite gravity measurements. *Global and Planetary Change*, *116*, 130–138.

456   https://doi.org/10.1016/j.gloplacha.2014.02.007

457   Chen, L., & Frauenfeld, O. W. (2016). Impacts of urbanization on future climate in China.

458   *Climate Dynamics*, *47*(1–2), 345–357. https://doi.org/10.1007/s00382-015-2840-6

459   Coutts, A. M., White, E. C., Tapper, N. J., Beringer, J., & Livesley, S. J. (2016). Temperature

460   and human thermal comfort effects of street trees across three contrasting street canyon

461   environments. *Theoretical and Applied Climatology*, *124*(1), 55–68.

462   https://doi.org/10.1007/s00704-015-1409-y

463   Dunne, J. P., Stouffer, R. J., & John, J. G. (2013). Reductions in labour capacity from heat stress

464   under climate warming. *Nature Climate Change*, *3*(6), 563–566.

465   https://doi.org/10.1038/nclimate1827

466   Epstein, S. A., Lee, S.-M., Katzenstein, A. S., Carreras-Sospedra, M., Zhang, X., Farina, S. C., et

467   al. (2017). Air-quality implications of widespread adoption of cool roofs on ozone and

468   particulate matter in southern California. *Proceedings of the National Academy of*

469   *Sciences*, *114*(34), 8991–8996. https://doi.org/10.1073/pnas.1703560114

470   Estrada, F., Botzen, W. J. W., & Tol, R. S. J. (2017). A global economic assessment of city

471   policies to reduce climate change impacts. *Nature Climate Change*, *7*(6), 403–406.

472   https://doi.org/10.1038/nclimate3301

473   Feng, W., Zhong, M., Lemoine, J.-M., Biancale, R., Hsu, H.-T., & Xia, J. (2013). Evaluation of

474   groundwater depletion in North China using the Gravity Recovery and Climate

475   Experiment (GRACE) data and ground-based measurements. *Water Resources Research*,

476   *49*(4), 2110–2118. https://doi.org/10.1002/wrcr.20192

477   Fischer, E. M., & Knutti, R. (2013). Robust projections of combined humidity and temperature

478   extremes. *Nature Climate Change*, *3*(2), 126–130. https://doi.org/10.1038/nclimate1682

479   Forzieri, G., Bianchi, A., Silva, F. B. e, Marin Herrera, M. A., Leblois, A., Lavalle, C., et al.

480   (2018). Escalating impacts of climate extremes on critical infrastructures in Europe.

481   *Global Environmental Change*, *48*, 97–107.

482   https://doi.org/10.1016/j.gloenvcha.2017.11.007

483   Gasparrini, A., Guo, Y., Hashizume, M., Lavigne, E., Zanobetti, A., Schwartz, J., et al. (2015).

484   Mortality risk attributable to high and low ambient temperature: a multicountry

485   observational study. *The Lancet*, *386*(9991), 369–375. https://doi.org/10.1016/S0140-

486   6736(14)62114-0

487   Georgescu, M., Morefield, P. E., Bierwagen, B. G., & Weaver, C. P. (2014). Urban adaptation

488   can roll back warming of emerging megapolitan regions. *Proceedings of the National*

489   *Academy of Sciences*, *111*(8), 2909–2914. https://doi.org/10.1073/pnas.1322280111

490   Guo, X., Huang, J., Luo, Y., Zhao, Z., & Xu, Y. (2017). Projection of heat waves over China for

491   eight different global warming targets using 12 CMIP5 models. *Theoretical and Applied*

492   *Climatology*, *128*(3), 507–522. https://doi.org/10.1007/s00704-015-1718-1

493   Harlan, S. L., Brazel, A. J., Prashad, L., Stefanov, W. L., & Larsen, L. (2006). Neighborhood

494   microclimates and vulnerability to heat stress. *Social Science & Medicine*, *63*(11), 2847–

495   2863. https://doi.org/10.1016/j.socscimed.2006.07.030

496   Heo, S., & Bell, M. L. (2018). Heat waves in South Korea: differences of heat wave

497   characteristics by thermal indices. *Journal of Exposure Science & Environmental*

498   *Epidemiology*, 1–16. https://doi.org/10.1038/s41370-018-0076-3

499   Heo, S., Bell, M. L., & Lee, J.-T. (2019). Comparison of health risks by heat wave definition:

500   Applicability of wet-bulb globe temperature for heat wave criteria. *Environmental*

501   *Research*, *168*, 158–170. https://doi.org/10.1016/j.envres.2018.09.032

502   Hu, K., Yang, X., Zhong, J., Fei, F., & Qi, J. (2017). Spatially Explicit Mapping of Heat Health

503   Risk Utilizing Environmental and Socioeconomic Data. *Environmental Science &*

504   *Technology*, *51*(3), 1498–1507. https://doi.org/10.1021/acs.est.6b04355

505   Hu, K., Guo, Y., Hochrainer-Stigler, S., Liu, W., See, L., Yang, X., et al. (2019). Evidence for

506   Urban-Rural Disparity in Temperature-Mortality Relationships in Zhejiang Province,

507   China. *Environmental Health Perspectives*, *127*(3), 37001.

508   https://doi.org/10.1289/EHP3556

509   Huang, J., Yu, H., Guan, X., Wang, G., & Guo, R. (2016). Accelerated dryland expansion under

510   climate change. *Nature Climate Change*, *6*(2), 166–171.

511   https://doi.org/10.1038/nclimate2837

512   Huang, K., Li, X., Liu, X., & Seto, K. C. (2019). Projecting global urban land expansion and heat

513   island intensification through 2050. *Environmental Research Letters*, *14*(11), 114037.

514   https://doi.org/10.1088/1748-9326/ab4b71

515   IEA. (2018). *The Future of Cooling: Opportunities for energy-efficient air conditioning*.

516   International Energy Agency. Retrieved from https://webstore.iea.org/the-future-of-

517   cooling

518   Im, E.-S., Pal, J. S., & Eltahir, E. A. B. (2017). Deadly heat waves projected in the densely

519   populated agricultural regions of South Asia. *Science Advances*, *3*(8), e1603322.

520   https://doi.org/10.1126/sciadv.1603322

521   Jackson, T. L., Feddema, J. J., Oleson, K. W., Bonan, G. B., & Bauer, J. T. (2010).

522   Parameterization of Urban Characteristics for Global Climate Modeling. *Annals of the*

523   *Association of American Geographers*, *100*(4), 848–865.

524   https://doi.org/10.1080/00045608.2010.497328

525   Kang, S., & Eltahir, E. A. B. (2018). North China Plain threatened by deadly heatwaves due to

526   climate change and irrigation. *Nature Communications*, *9*(1), 1–9.

527   https://doi.org/10.1038/s41467-018-05252-y

528   Knauer, J., El-Madany, T. S., Zaehle, S., & Migliavacca, M. (2018). Bigleaf—An R package for

529   the calculation of physical and physiological ecosystem properties from eddy covariance

530   data. *PLOS ONE*, *13*(8), e0201114. https://doi.org/10.1371/journal.pone.0201114

531   Krayenhoff, E. S., Moustaoui, M., Broadbent, A. M., Gupta, V., & Georgescu, M. (2018).

532   Diurnal interaction between urban expansion, climate change and adaptation in US cities.

533   *Nature Climate Change*, *8*(12), 1097. https://doi.org/10.1038/s41558-018-0320-9

534   Laaidi, K., Zeghnoun, A., Dousset, B., Bretin, P., Vandentorren, S., Giraudet, E., & Beaudeau, P.

535   (2011). The Impact of Heat Islands on Mortality in Paris during the August 2003 Heat

536   Wave. *Environmental Health Perspectives*, *120*(2), 254–259.

537   https://doi.org/10.1289/ehp.1103532

538   Lee, D. O. (1991). Urban—rural humidity differences in London. *International Journal of*

539   *Climatology*, *11*(5), 577–582. https://doi.org/10.1002/joc.3370110509

540   Lee, X. (2018). *Fundamentals of Boundary-Layer Meteorology*. Springer International

541   Publishing. Retrieved from https://www.springer.com/gp/book/9783319608518

542   Li, D., Bou-Zeid, E., & Oppenheimer, M. (2014). The effectiveness of cool and green roofs as

543   urban heat island mitigation strategies. *Environmental Research Letters*, *9*(5), 055002.

544   https://doi.org/10.1088/1748-9326/9/5/055002

545   Li, J., Chen, Y. D., Gan, T. Y., & Lau, N.-C. (2018). Elevated increases in human-perceived

546   temperature under climate warming. *Nature Climate Change*, *8*(1), 43–47.

547   https://doi.org/10.1038/s41558-017-0036-2

548   Lucas, R. A. I., Epstein, Y., & Kjellstrom, T. (2014). Excessive occupational heat exposure: a

549   significant ergonomic challenge and health risk for current and future workers. *Extreme*

550   *Physiology & Medicine*, *3*(1), 14. https://doi.org/10.1186/2046-7648-3-14

551   Luo, M., & Lau, N.-C. (2019). Urban Expansion and Drying Climate in an Urban Agglomeration

552   of East China. *Geophysical Research Letters*, *46*(12), 6868–6877.

553   https://doi.org/10.1029/2019GL082736

554   Matthews, T. K. R., Wilby, R. L., & Murphy, C. (2017). Communicating the deadly

555   consequences of global warming for human heat stress. *Proceedings of the National*

556   *Academy of Sciences*, *114*(15), 3861–3866. https://doi.org/10.1073/pnas.1617526114

557   Miao, S., & Chen, F. (2014). Enhanced modeling of latent heat flux from urban surfaces in the

558   Noah/single-layer urban canopy coupled model. *Science China Earth Sciences*, *57*(10),

559   2408–2416. https://doi.org/10.1007/s11430-014-4829-0

560   Monteith, J., & Unsworth, M. (2013). *Principles of Environmental Physics: Plants, Animals, and*

561   *the Atmosphere* (4 edition). Academic Press.

562   Murage, P., Hajat, S., & Kovats, R. S. (2017). Effect of night-time temperatures on cause and

563   age-specific mortality in London. *Environmental Epidemiology*, *1*(2), e005.

564   https://doi.org/10.1097/EE9.0000000000000005

565   Murakami, D., & Yamagata, Y. (2019). Estimation of Gridded Population and GDP Scenarios

566   with Spatially Explicit Statistical Downscaling. *Sustainability*, *11*(7), 2106.

567   https://doi.org/10.3390/su11072106

568   Myers, N., Mittermeier, R. A., Mittermeier, C. G., da Fonseca, G. A. B., & Kent, J. (2000).

569   Biodiversity hotspots for conservation priorities. *Nature*, *403*(6772), 853–858.

570   https://doi.org/10.1038/35002501

571   Obradovich, N., Migliorini, R., Mednick, S. C., & Fowler, J. H. (2017). Nighttime temperature

572   and human sleep loss in a changing climate. *Science Advances*, *3*(5), e1601555.

573   https://doi.org/10.1126/sciadv.1601555

574   Oke, T. R. (1982). The energetic basis of the urban heat island. *Quarterly Journal of the Royal*

575   *Meteorological Society*, *108*(455), 1–24. https://doi.org/10.1002/qj.49710845502

576   Pal, J. S., & Eltahir, E. A. B. (2016). Future temperature in southwest Asia projected to exceed a

577   threshold for human adaptability. *Nature Climate Change*, *6*(2), 197–200.

578   https://doi.org/10.1038/nclimate2833

579   Patel, T., Mullen, S. P., & Santee, W. R. (2013). Comparison of Methods for Estimating Wet-

580   Bulb Globe Temperature Index From Standard Meteorological Measurements. *Military*

581   *Medicine*, *178*(8), 926–933. https://doi.org/10.7205/MILMED-D-13-00117

582   Raymond, C., Singh, D., & Horton, R. M. (2017). Spatiotemporal Patterns and Synoptics of

583   Extreme Wet-Bulb Temperature in the Contiguous United States. *Journal of Geophysical*

584   *Research: Atmospheres*, *122*(24), 13,108-13,124. https://doi.org/10.1002/2017JD027140

585 Raymond, Colin, Matthews, T., & Horton, R. M. (2020). The emergence of heat and humidity

586   too severe for human tolerance. *Science Advances*, *6*(19), eaaw1838.

587   https://doi.org/10.1126/sciadv.aaw1838

588 Rohat, G., Flacke, J., Dosio, A., Dao, H., & Maarseveen, M. van. (2019). Projections of Human

589   Exposure to Dangerous Heat in African Cities Under Multiple Socioeconomic and

590   Climate Scenarios. *Earth's Future*, *7*(5), 528–546.

591   https://doi.org/10.1029/2018EF001020

592 Seto, K. C., Güneralp, B., & Hutyra, L. R. (2012). Global forecasts of urban expansion to 2030

593   and direct impacts on biodiversity and carbon pools. *Proceedings of the National*

594   *Academy of Sciences*, *109*(40), 16083–16088. https://doi.org/10.1073/pnas.1211658109

595 Sherwood, S. C., & Huber, M. (2010). An adaptability limit to climate change due to heat stress.

596   *Proceedings of the National Academy of Sciences*, *107*(21), 9552–9555.

597   https://doi.org/10.1073/pnas.0913352107

598 Skamarock, C., Klemp, B., Dudhia, J., Gill, O., Barker, D., Duda, G., et al. (2008). A Description

599   of the Advanced Research WRF Version 3. https://doi.org/10.5065/D68S4MVH

600 Smith, A., Lott, N., & Vose, R. (2011). The Integrated Surface Database: Recent Developments

601   and Partnerships. *Bulletin of the American Meteorological Society*, *92*(6), 704–708.

602   https://doi.org/10.1175/2011BAMS3015.1

603 Stone, B. (2012). *The City and the Coming Climate: Climate Change in the Places We Live* (1

604   edition). New York: Cambridge University Press.

605 Stone, B., Vargo, J., Liu, P., Habeeb, D., DeLucia, A., Trail, M., et al. (2014). Avoided Heat-

606   Related Mortality through Climate Adaptation Strategies in Three US Cities. *PLoS ONE*,

607   *9*(6), e100852. https://doi.org/10.1371/journal.pone.0100852

608 Um, H.-H., Ha, K.-J., & Lee, S.-S. (2007). Evaluation of the urban effect of long-term relative

609   humidity and the separation of temperature and water vapor effects. *International Journal*

610   *of Climatology*, *27*(11), 1531–1542. https://doi.org/10.1002/joc.1483

611 UN DESA. (2014). *World Urbanization Prospects: The 2014 Revision, Highlights*. New York:

612   United Nations, Department of Economic and Social Affairs, Population Division.

613   Retrieved from http://esa.un.org/unpd/wup/highlights/wup2014-highlights.pdf

614 Underwood, B. S., Guido, Z., Gudipudi, P., & Feinberg, Y. (2017). Increased costs to US

615   pavement infrastructure from future temperature rise. *Nature Climate Change*, *7*(10),

616   704–707. https://doi.org/10.1038/nclimate3390

617 Vuuren, D. P. van, Edmonds, J., Kainuma, M., Riahi, K., Thomson, A., Hibbard, K., et al.

618   (2011). The representative concentration pathways: an overview. *Climatic Change*,

619   *109*(1–2), 5–31. https://doi.org/10.1007/s10584-011-0148-z

620 Wang, Z.-H., Zhao, X., Yang, J., & Song, J. (2016). Cooling and energy saving potentials of

621   shade trees and urban lawns in a desert city. *Applied Energy*, *161*, 437–444.

622   https://doi.org/10.1016/j.apenergy.2015.10.047

623 Williams, N. S. G., Lundholm, J., & MacIvor, J. S. (2014). FORUM: Do green roofs help urban

624   biodiversity conservation? *Journal of Applied Ecology*, *51*(6), 1643–1649.

625   https://doi.org/10.1111/1365-2664.12333

626 Yang, B., Yang, X., Leung, L. R., Zhong, S., Qian, Y., Zhao, C., et al. (2019). Modeling the

627   Impacts of Urbanization on Summer Thermal Comfort: The Role of Urban Land Use and

628   Anthropogenic Heat. *Journal of Geophysical Research: Atmospheres*, *124*(13), 6681–

629   6697. https://doi.org/10.1029/2018JD029829

630   Yang, J., Wang, Z.-H., Chen, F., Miao, S., Tewari, M., Voogt, J. A., & Myint, S. (2015).

631   Enhancing Hydrologic Modelling in the Coupled Weather Research and Forecasting–

632   Urban Modelling System. *Boundary-Layer Meteorology*, *155*(1), 87–109.

633   https://doi.org/10.1007/s10546-014-9991-6

634   Yang, J., Wang, Z.-H., & Kaloush, K. E. (2015). Environmental impacts of reflective materials:

635   Is high albedo a 'silver bullet' for mitigating urban heat island? *Renewable and*

636   *Sustainable Energy Reviews*, *47*, 830–843. https://doi.org/10.1016/j.rser.2015.03.092

637   Zhao, L., Lee, X., & Schultz, N. M. (2017). A wedge strategy for mitigation of urban warming in

638   future climate scenarios. *Atmospheric Chemistry and Physics*, *17*(14), 9067–9080.

639   https://doi.org/10.5194/acp-17-9067-2017

640   Zinzi, M., & Agnoli, S. (2012). Cool and green roofs. An energy and comfort comparison

641   between passive cooling and mitigation urban heat island techniques for residential

642   buildings in the Mediterranean region. *Energy and Buildings*, *55*, 66–76.

643   https://doi.org/10.1016/j.enbuild.2011.09.024

644

645
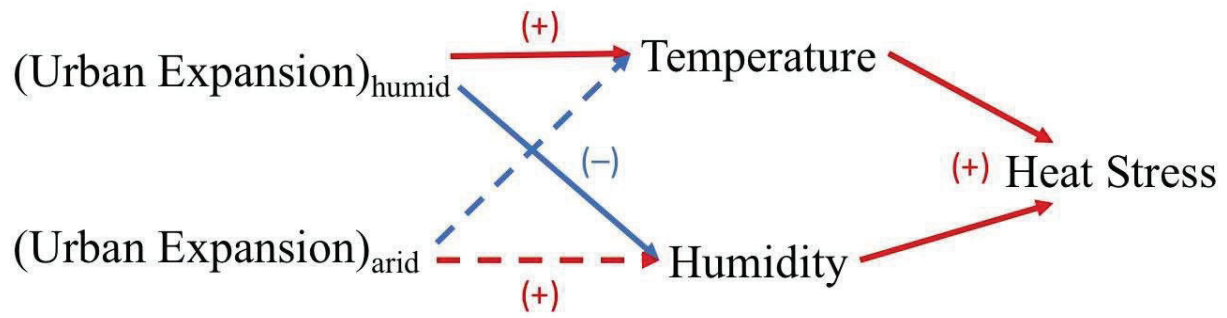
646
647 **Figure 1** Mechanisms of urban expansion affecting heat stress, in humid and arid climates.
648
649
650
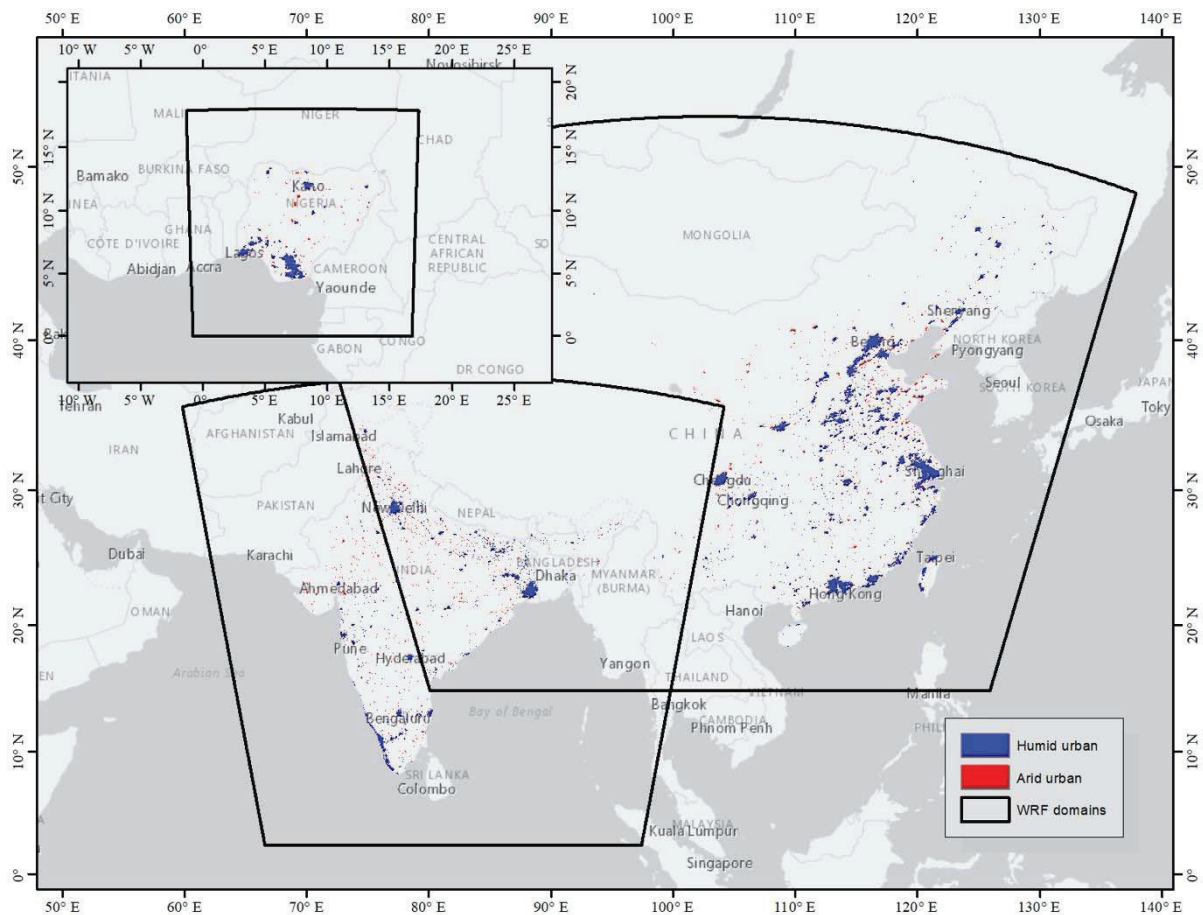
651
652 **Figure 2** The domains for the Weather Research and Forecasting (WRF) simulations and the
653 geographic distributions of humid and arid urban areas in China, India, and Nigeria.
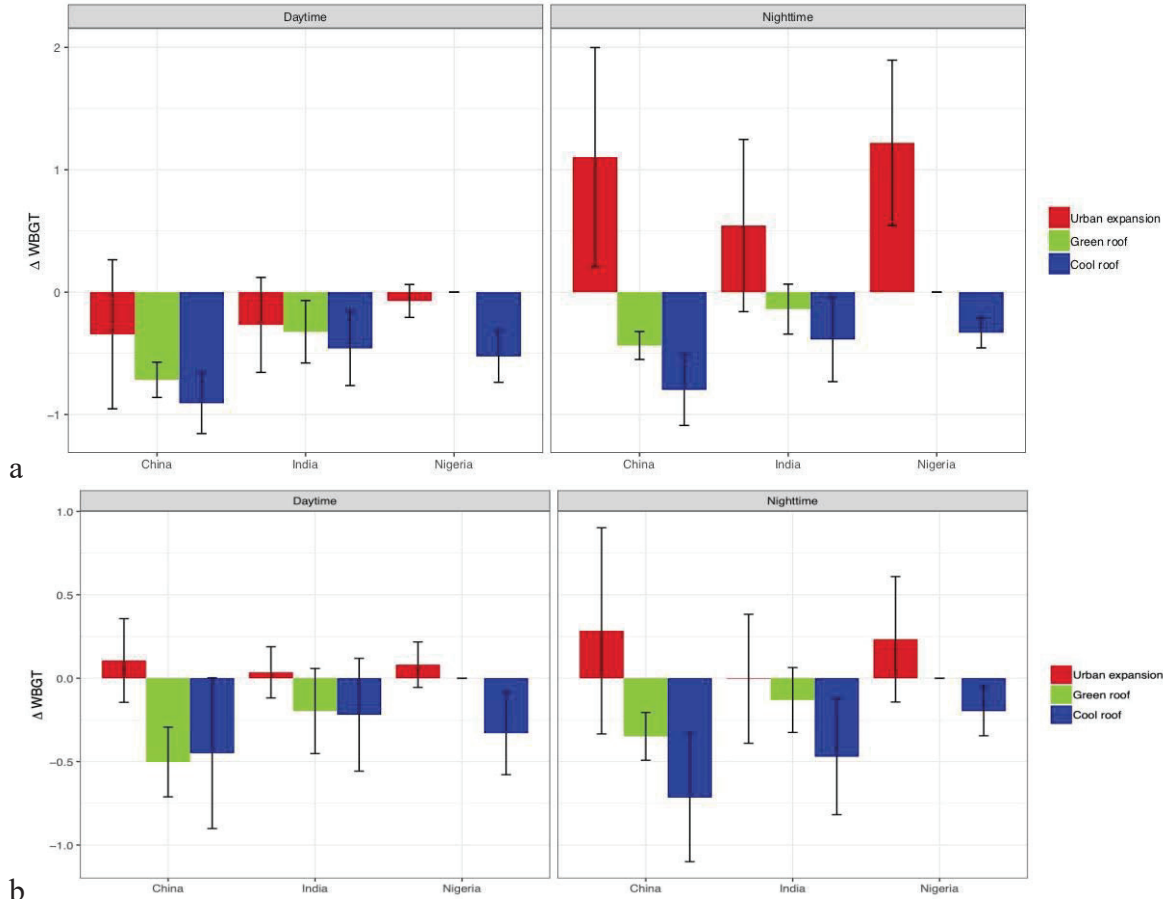
654

655   a

656   b
657   **Figure 3** Summer average changes in wet-bulb globe temperature (WBGT) in humid (a) and arid
658   (b) urban lands, due to urban land expansion and heat island mitigations. Urban heat island
659   mitigation measures include installing green and cool roofs, and the changes are calculated using
660   urban land expansion scenario as the baseline. Error bars represent one standard deviation from
661   the regional means.
662

663
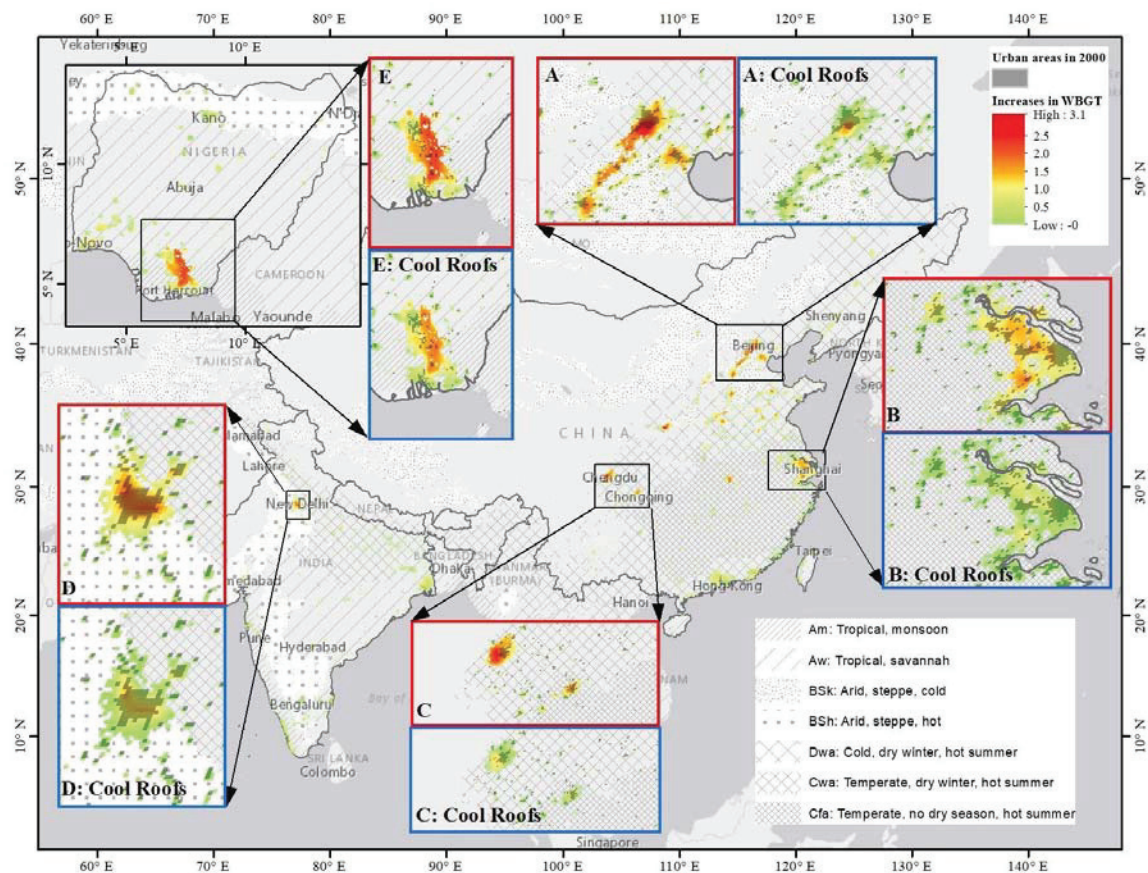
664
665 **Figure 4** Geographic distributions of changes in nighttime wet-bulb globe temperature (WBGT)
666 due to urban expansion. Enlarged maps with red frames show five mega urban regions
667 with >2°C warming: A) Beijing-Tianjin-Hebei, B) Yangtze River Delta, C) Chengdu-
668 Chongqing, D) Delhi Metropolitan Area, and E) Port Harcourt, and those with blue frames show
669 the respective warming with installment of cool roofs. (Base map credits: ESRI, HERE, Garmin,
670 © OpenStreetMap contributors, and the GIS user community.)
671

672

673
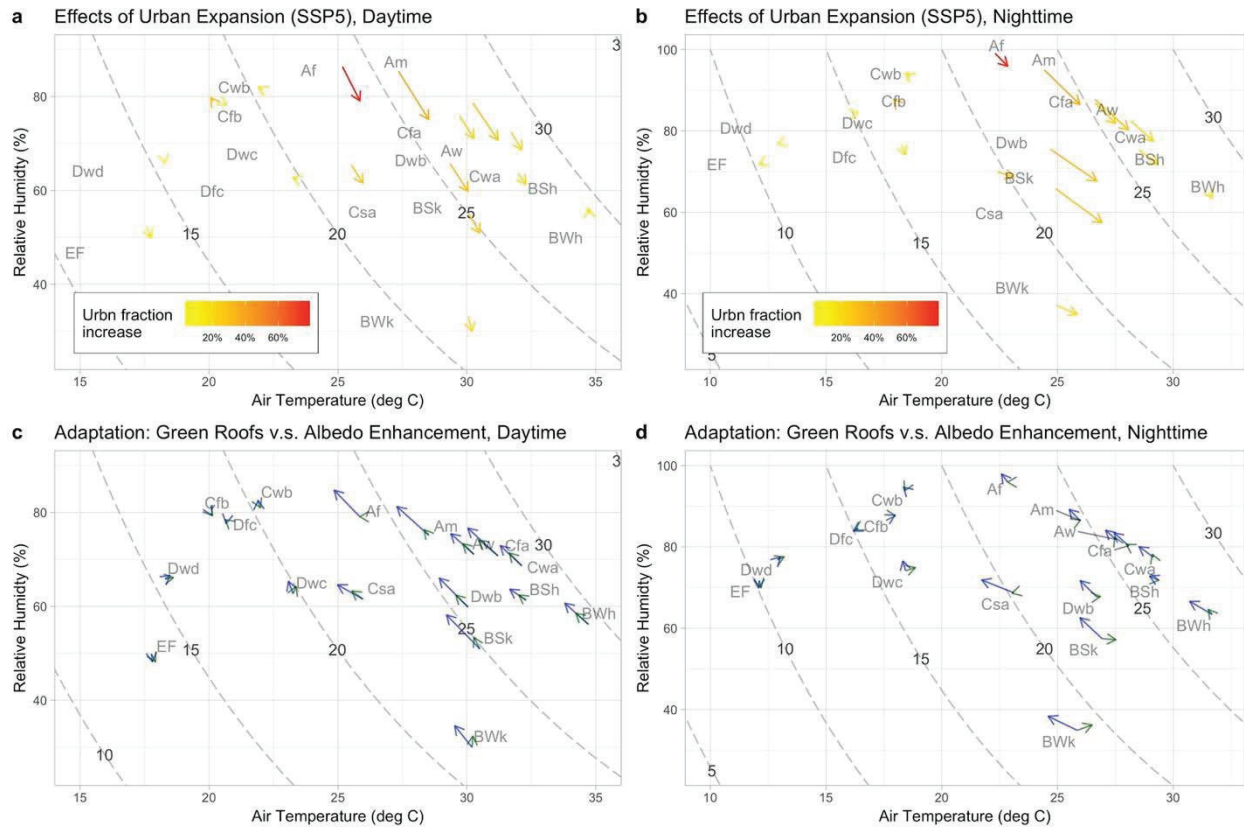
Figure 5 Effects of urban land expansion (a-b) and heat mitigation (c-d) on air temperature (x-axis), relative humidity (y-axis), and wet-bulb globe temperature (WBGT, black dashed curves), during daytime (a and c) and nighttime (b and d), in future climate conditions (2049–2054, RCP8.5). Arrows represent the average effects of urban grids within the same Köppen climate zones[49]: in a-b heads and tails are conditions of before and after land urban expansion, and in c-d heads and tails are without and with urban heat island mitigation measures. In c-d, green arrows represent the effects of installing green roofs and blue ones represent those of cool roofs. Köppen climates notations: A-tropical, B-arid, C-temperate, D-cold, W: desert, S: steppe, h: hot, k: cold, m-monsoon, w-dry winter, s-dry summer, f-no dry season, a-hot summer, b-warm summer, c-cold summer.

684 **Table 1** Changes in air temperature and specific humidity due to urban expansion during
685 daytime and nighttime, in different climate zones.

Climate zone	Air temperature (°C)		Specific humidity (g/kg)		Percentage of total urban area in 2050
	Daytime	Nighttime	Daytime	Nighttime	
Am: Tropical, monsoon	1.30	1.72	-1.25	0.00	7%
Aw: Tropical, savannah	0.58	0.91	-0.65	-0.12	23%
BSh: Arid, steppe, hot	0.33	0.87	-0.46	-0.08	8%
BSk: Arid, steppe, cold	0.47	2.13	-0.73	-0.04	5%
Cfa: Temperate, no dry season, hot summer	1.02	1.55	-1.08	-0.03	14%
Cwa: Temperate, dry winter, hot summer	0.45	1.02	-0.57	-0.06	26%
Dwb: Cold, dry winter, warm summer	0.76	2.15	-6.73	0.14	14%

686

687 **Table 2** Average GDP per capita (PPP, USD 2005/year) in the five mega-urban regions (MURs).

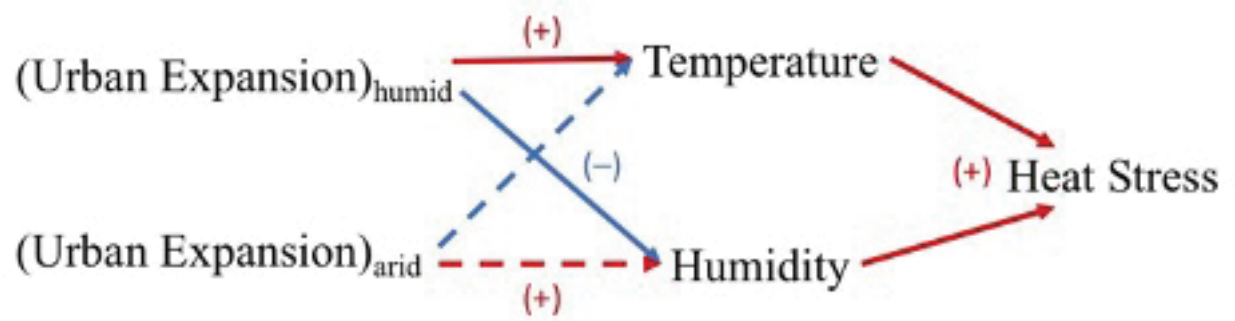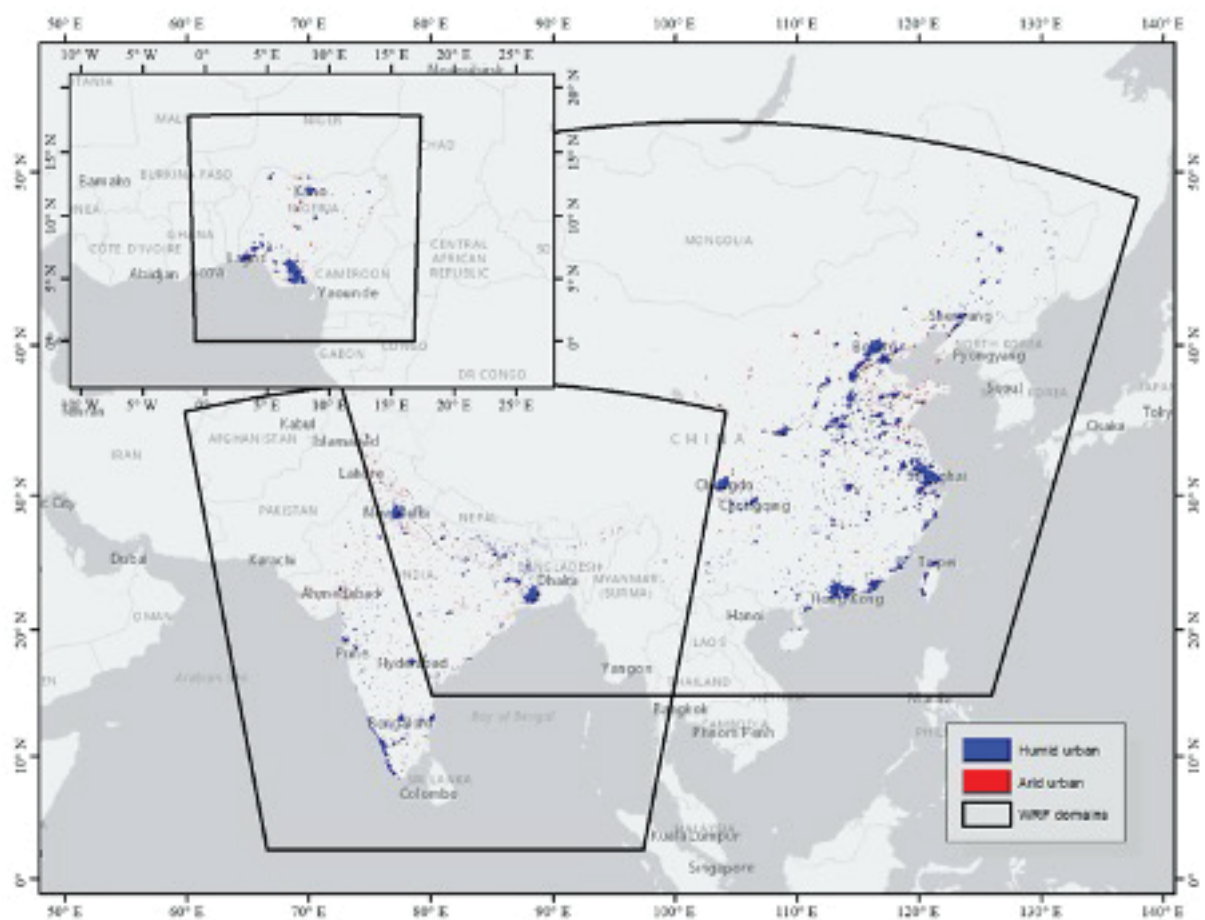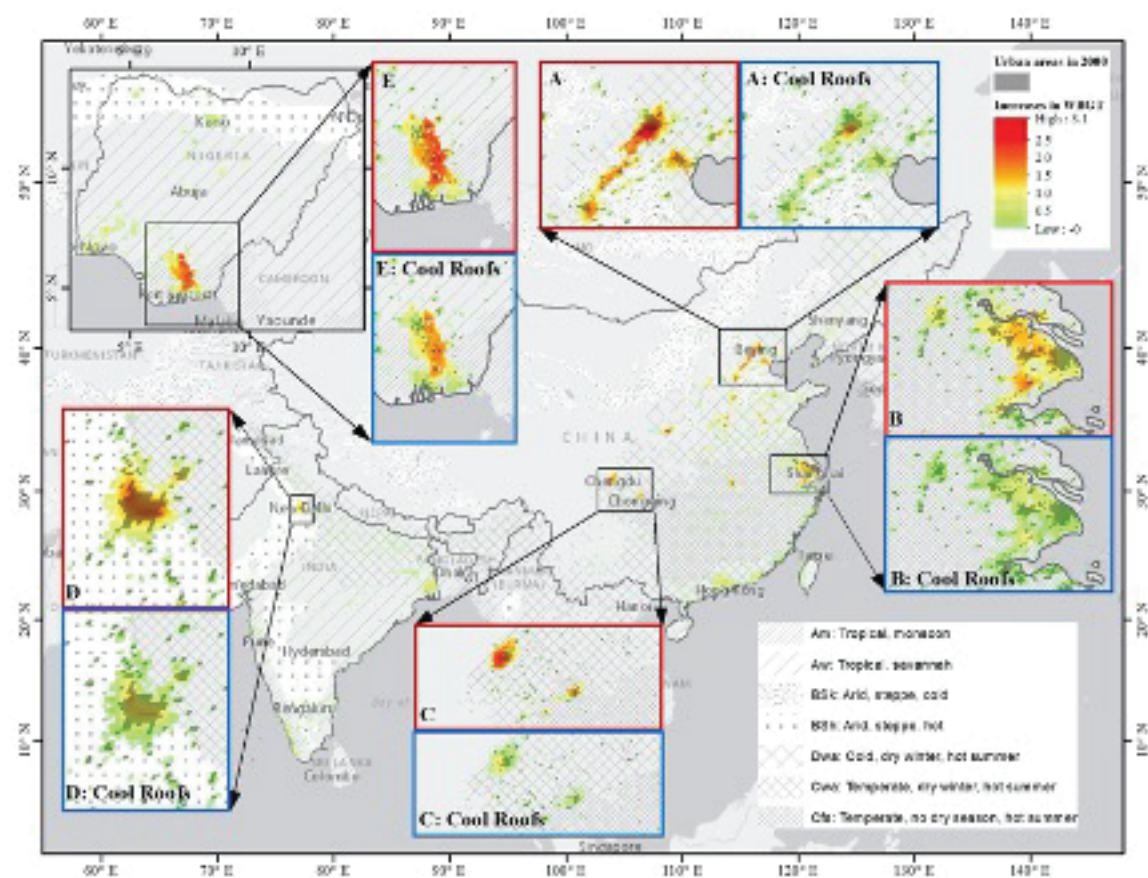| MUR	GDP per capita (PPP, USD 2005)
Beijing-Tianjin-Hebei	33,024
Yangtze-River-Delta	42,843
Chengdu-Chongqing	31,592
Delhi Metropolitan Area	15,577
Port Harcourt	10,187

688
689

Figure 1.

Figure 2.

Figure 4.

Figure 5.

a Effects of Urban Expansion (SSP5), Daytime

b Effects of Urban Expansion (SSP5), Nighttime

c Adaptation: Green Roofs v.s. Albedo Enhancement, Daytime

d Adaptation: Green Roofs v.s. Albedo Enhancement, Nighttime

Figure 3.

a

b